

SPECTRAL ANALYSIS OF THE OPTICAL CONTINUUM IN THE 24 APRIL 1981 FLARE

DONALD F. NEIDIG

Air Force Geophysics Laboratory, Sacramento Peak Observatory, Sunspot, NM 88349, U.S.A.*

(Received 17 March; in revised form 7 September, 1982)

Abstract. Spectrograph and multiple-band polarimeter observations of the 24 April 1981 white-light flare indicate the presence of an optical continuum with intensity increasing strongly below 4000 Å. The flare emission (lines and continuum combined) is unpolarized and, at 3600 Å, exceeds the brightness of the background solar surface by 360%. Analysis of the spectrum between 3600 and 8200 Å, at a location three arc sec from the brightest point in the kernel, yields a probable temperature of 6700 K for the continuum emitting layer. The wavelength dependence of the continuum indicates emission by both negative hydrogen (H^-) and Balmer continuum, with the H^- probably originating in the upper photosphere at a height (above $\tau_{5000 \text{ Å}} = 1$) in the range 200–300 km. Analysis of the Balmer lines and continuum yields an electron density $5.3 \times 10^{13} \text{ cm}^{-3}$ and a second-level hydrogen column density $1.1 \times 10^{16} \text{ cm}^{-2}$. The peak radiative output integrated over wavelength is $6.1 \times 10^{27} \text{ erg s}^{-1}$. The observed continuum intensity, if originating at a height of 300 km, implies an energy loss rate of $10^3 \text{ erg s}^{-1} \text{ cm}^{-3}$.

1. Introduction

At least 47 flares have now been observed which contain optical continuum as determined by visual, spectrographic, or broad-band photographic observations (see references within). Such white-light flares (WLF) are among the most powerful of flares, and radiate as much as $10^{28} \text{ erg s}^{-1}$ in the optical continuum alone. Thus, the optical continuum constitutes a major term in the peak power budget of such flares, and, in addition, fixes the location and depth of deposition of a significant fraction of the flare energy. Previous studies of WLFs have placed the source of the optical continuum in the low temperature, high density regime of the flare: the low photosphere (Najita and Orrall, 1970); the upper photosphere (Švestka, 1970; Machado, 1971; Machado and Rust, 1974; Hiei, 1982); the low chromosphere (Švestka, 1966a; Hudson, 1972; Lin and Hudson, 1976). It is possible that all these layers in the solar atmosphere contribute, to some degree, to the continuum in WLFs and that several emission processes may be involved, the relative importances of which may vary from one flare to another. Although the range of heights in the atmosphere of the suggested sites for the optical continuum is only 500 km, the total atmospheric column density varies by a large factor (approximately two orders of magnitude (e.g. Vernazza *et al.*, 1981) over the same range. Hence the determination of the height of the continuum-emitting layers in a particular flare is essential to understanding the processes by which the flare energy is deposited in, or transported through, the atmosphere. This would be particularly true if, as is commonly assumed, the entire quantity of the flare energy is released in the corona and

* Operated by the Association of Universities for Research in Astronomy, Inc., under contract with the National Science Foundation.

subsequently transported to the lower atmosphere by heat conduction or high energy particles.

Aside from the energetics the data presented herein may also provide an understanding of the 'blue continuum' observed in a number of WLFs (Švestka, 1966b, 1976; Zirin, 1980) which presumably is the cause of the bluish color noted in visual observations of WLFs. Zirin (1980) and Zirin and Neidig (1981) described the blue continuum as distinct from Balmer continuum and possibly due to some unidentified source of opacity, although the present observations show that emission by negative hydrogen alone may be sufficient, at least in the case of the 24 April flare.

This paper will describe and interpret the observational data pertaining to the spectrum of the optical continuum at peak intensity in the 24 April flare. Morphology, timing, and relationships to X-ray and microwave emissions will be deferred to a future study. Section 2 describes the observations and establishes the spectral similarity of the 24 April flare to other WLFs. Section 3 contains the analysis of the continuum, and leads to a determination of the optical thickness, radiative source function, and electron density in the flare. Section 4 discusses the validity of the methods used, the reality of the blue continuum, and the probable height in the atmosphere of the continuum-emitting layer. The flare energetics are summarized in Section 5.

2. Observations

2.1. THE 24 APRIL 1981 FLARE

Figure 1 shows the flare at maximum brightness (importance 2B, location N 18 W 50) as photographed at 3610 and 4275 Å with the multiband polarimeter (MBP) at Sacramento Peak Observatory. The MBP (designed by J. M. Beckers) provides a photographic record in five wavelength/bandpasses at 3610/22, 4275/40, 4957/48, 5645/50, and 6203/49 Å, each in two simultaneously obtained orthogonal planes of linear polarization. The 5645 Å channel is recorded a second time during the cycle, but with a 45 degree rotation in the polarizing planes. Time resolution at 5646 Å during the present observations was 15 s (30 s for the complete cycle). As in the flare of 1 July 1980 (Zirin and Neidig, 1981) the emission showed no measurable linear polarization in any of the five channels. The brightness peaked in a broad maximum near 13:57 UT, with enhancements $\Delta I/I_{\text{ph}}$ of 3.6 (3610 Å), 0.65 (4275 Å), and 0.40 (6203 Å), where I_{ph} is the intensity of the undisturbed photosphere adjacent to the flare, away from the bright photospheric network.

A series of spectrograms was obtained from the Universal Spectrograph, covering a large spectral range in a cycle of three exposures in third order (3550–4550 Å), second order (4400–5920 Å), and first order (5850–9100 Å). Time between exposures was 5 s. Spectral resolutions ($\lambda/\Delta\lambda$) in third, second and first orders are 5.1×10^5 , 3.4×10^5 , and 1.7×10^5 , respectively, with dispersions of 1.6, 2.3, and 5.3 Å mm^{-1} . In the present observations, however, the actual minimum resolvable interval $\Delta\lambda$ was set by a 0.045 mm entrance slit resulting in $\Delta\lambda$'s of 0.07, 0.10, and 0.24 Å. The spectrograph data

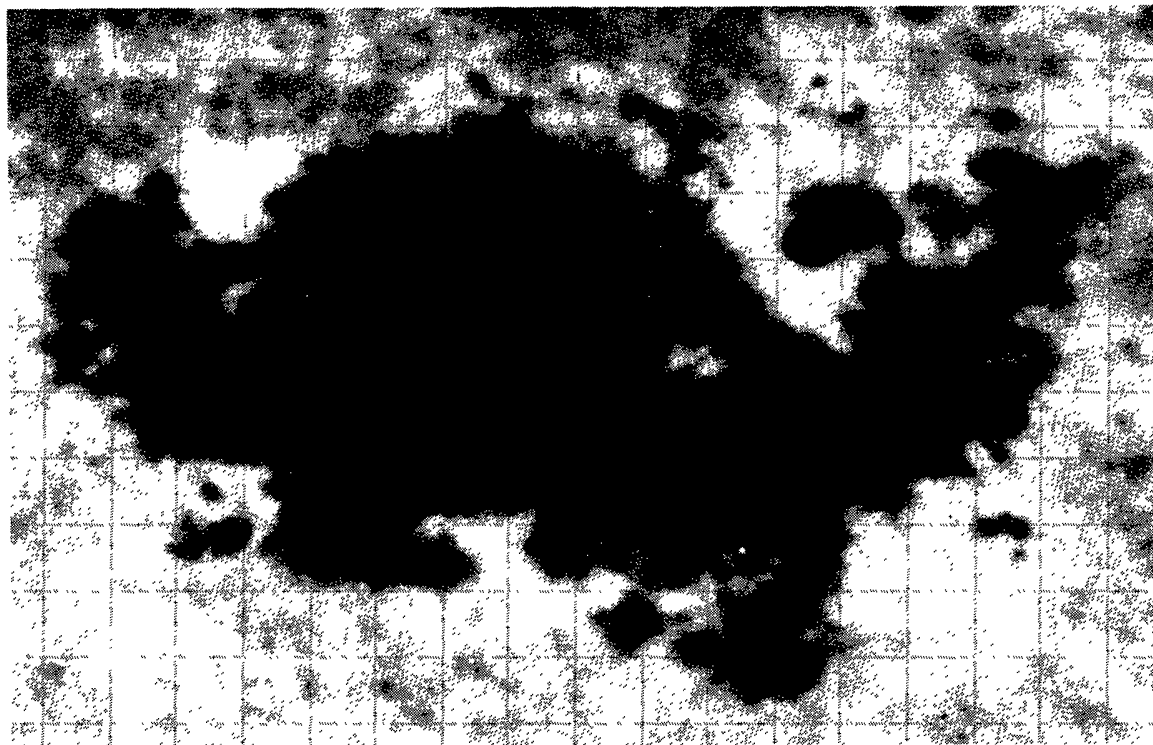
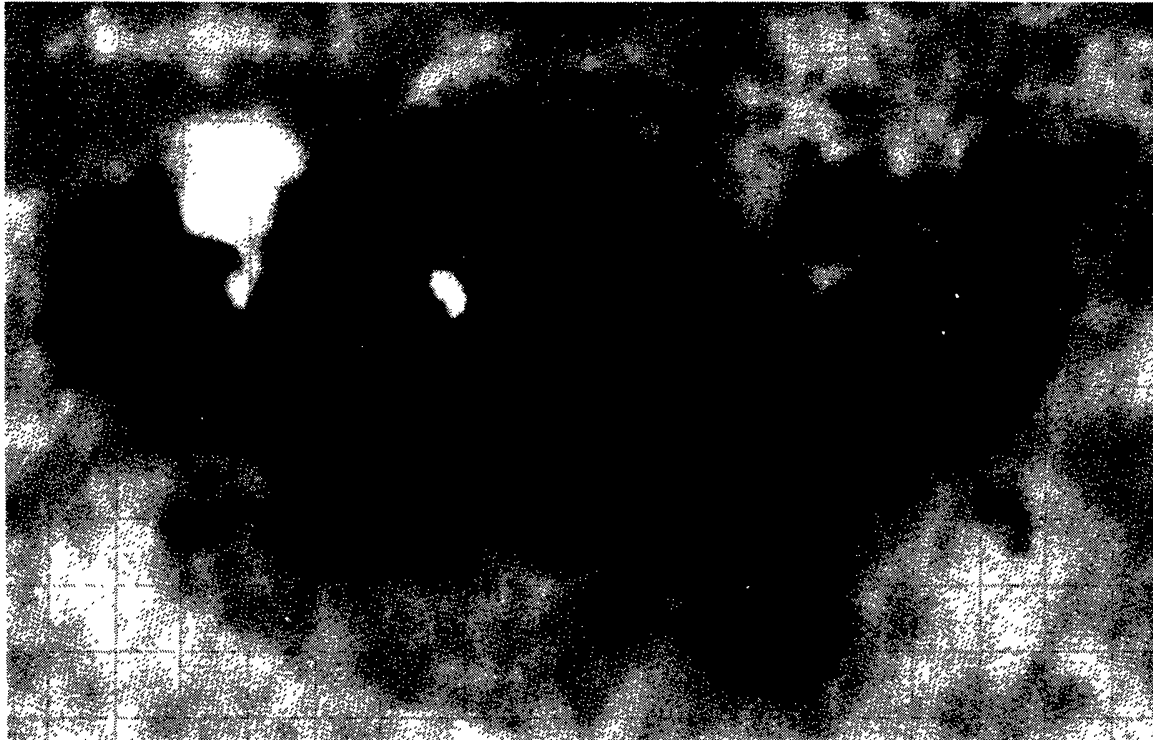


Fig. 1. The flare at peak brightness (13:57 UT) photographed with the Multiband Polarimeter at 3610 Å (*top*) and 4275 Å (*bottom*). The soft focus in the 3610 Å image is due to chromatic aberration. West is at the top, north to the left. The long dimension of the sunspot complex is 133 arc sec. Note the second, smaller kernel in the 3610 Å image, which does not appear at 4275 Å.

cover the time of peak intensity in the flare, although—and this is important to remember throughout the entire discussion—the slit was positioned about three arcsec east of the brightest point in the kernel. This location, nevertheless, lies outside the sunspot penumbra, a circumstance which considerably facilitates the subtraction of the background spectrum. The spectrograms used in the analysis were taken at 13:56:47, 13:56:52, and 13:56:57 UT, in third, second, and first order, respectively. A portion of the third-order spectrogram is shown in Figure 2.

The width of the continuum on the spectrograms is 0.7 mm (14 arc sec) as determined from microdensitometer scans made in a direction perpendicular to the dispersion. A slit length of 0.20 mm was used in the scans made parallel to the dispersion; this results in a measured intensity such that the intensity difference $\Delta I = I_{f,\lambda} - I_{0,\lambda}$ is six percent less than would have been obtained had the scan been made at the actual peak of the flare emission. No correction for this effect has been made herein. The background intensity in the spectrum was measured from scans made in the quiet photosphere adjacent to the flare, away from the bright network (location immediately above the continuum strip in Figure 2).

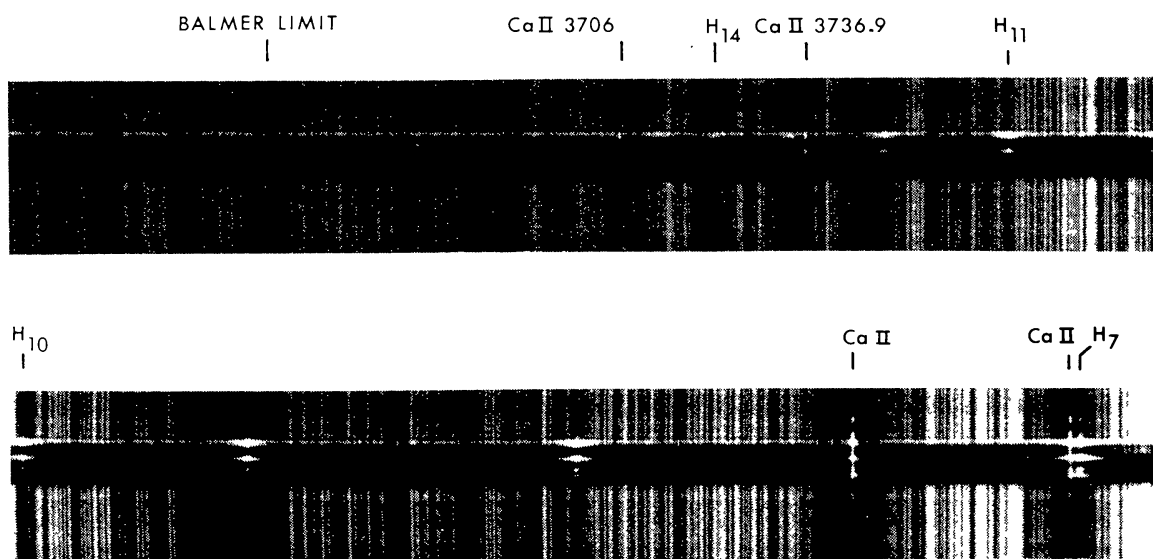


Fig. 2. A portion of the flare spectrum showing the continuum and highly broadened members of the Balmer series.

The flare spectrum shows Balmer lines which are exceedingly broad and intense. For $H\alpha$ the intensity $(I_{f,H\alpha} - I_{0,H\alpha \pm 15 \text{ \AA}}) / I_{0,H\alpha \pm 15 \text{ \AA}} = 2.5$ at line center, with a full width exceeding 30 \AA between the points of zero enhancement; this corresponds to an equivalent width in emission of approximately 18 \AA . The higher Balmer lines (Figure 2) merge below H_{16} to form a strong continuum which is superposed on another, weaker continuum visible at longer wavelengths and which extends beyond the range of the spectrograph ($\lambda > 9100 \text{ \AA}$). Intensity measurements, made in a number of bright windows in the spectrum between 3600 and 4000 \AA (Figure 3, top), show both of these continuum components in the flare spectrum. The probable source of the weaker

continuum is emission by the negative hydrogen ion (H^-), as can be easily concluded by comparing the competing processes (H^- , hydrogen free-free, and hydrogen free-bound transitions) under conditions characteristic of the lower chromosphere in flares (e.g., Jefferies and Orrall, 1961; Hiei, 1982). Emission by hydrogen free-free transitions is weaker by approximately two orders of magnitude than H^- (at 7000 K and electron density 10^{13} cm^{-3}). As for Paschen and higher continua it is noted that the total emission by these contributors will be approximately 1/60 that of the Balmer continuum (at 7000 K). The observations in Figure 3, however, indicate the weak continuum in the 24 April flare to be 1/4 the intensity of the Balmer continuum; hence the only important contributor to the weak continuum must be H^- , as was concluded also by Hiei (1982) for the WLF of 10 September, 1974. This conclusion is only tentative, however, as it does not rule out the possibility of additional sources of opacity which might become effective in a flaring atmosphere (further discussion on this point is contained in Section 4).

2.2. PREVIOUS OBSERVATIONS OF WLFs

The strong contrast of the optical continuum at short wavelengths is a characteristic of many WLFs, as is readily apparent in the observations made with broad-band filters. MBP measurements in the flare of 1 July, 1980 (Zirin and Neidig, 1981) yielded $\Delta I/I_{\text{ph}} \simeq 1.5$ at 3610 Å, with $\Delta I/I_{\text{ph}} \lesssim 0.20$ in all channels longward of 4200 Å; an additional measurement at 3862 Å (20 Å band), obtained from Big Bear Solar Observatory, yielded $\Delta I/I_{\text{ph}} = 1.0$. Zirin (1980) observed strong enhancements ($\Delta I/I_{\text{ph}} \simeq 1$) at 3835 Å (64 Å band) in several flares in which the corresponding enhancements at longer wavelengths were weak or absent. The latter enhancements were apparently not due to emission in the H_α line (Zirin, 1980) and are probably similar to the 'flashes' observed at 3835 Å in the 2 August, 1972 flare (Zirin and Tanaka, 1973).

Some additional, although less reliable, information on the spectral distribution of WLF continua can be obtained from single-channel data by comparing $\Delta I/I_{\text{ph}}$ measurements for two groups of flares—those observed in effective wavelengths shortward of (for example) 4500 Å and those observed longward of 4500 Å. The former group includes five WLFs observed on blue sensitive photographs by Slonim and Korobova (1975), where $\lambda_{\text{eff}} = 4100 \text{ Å}$, and one by Waldmeier (1958), where $\lambda_{\text{eff}} = 4200 \text{ Å}$. The second group includes two flares observed in a spectrogram at $\lambda \geq 6200 \text{ Å}$ (Ellison, 1946; Ellison and Conway, 1950), three in a broad band filter at 5800 Å (DeMastus and Stover, 1967; McIntosh and Donnelly, 1972) and one flare at both 4950 and 5900 Å in broad band filters (Rust and Hegwer, 1975). The mean values of $\Delta I/I_{\text{ph}}$ for the first and second groups are 0.71 and 0.14, respectively, indicating the increased contrast at shorter wavelengths. It should be emphasized that all measurements of $\Delta I/I_{\text{ph}}$ made over broad spectral ranges represent upper limits for the actual flare optical continua, as contributions from line emissions might be included in the total intensity. This is particularly relevant to the study of the blue continuum because the number of spectral lines per unit wavelength interval increases strongly at short wavelengths.

Spectrographic data on WLFs, although scarce, have also shown the increase in

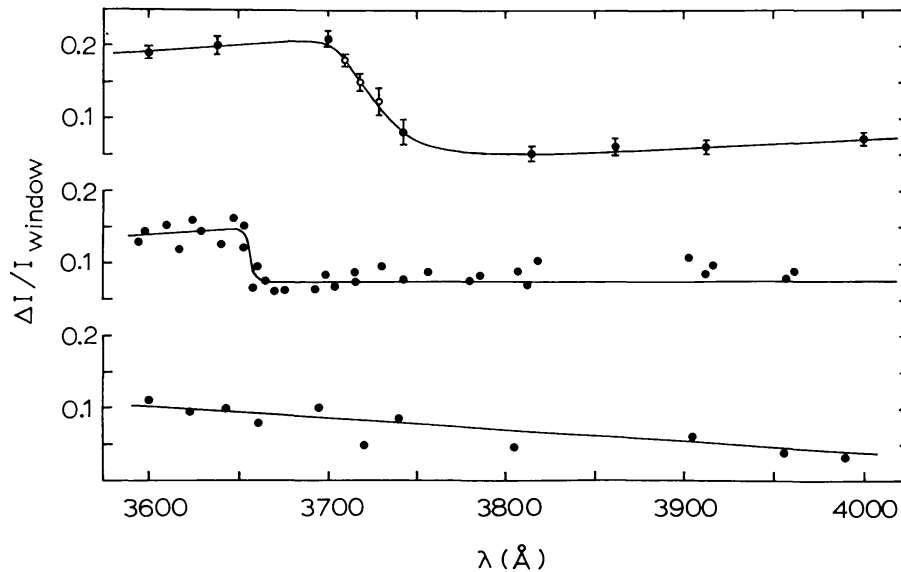


Fig. 3. A comparison of the intensity enhancements in spectral windows for three WLFs (*Top*: 24 April, 1981. *Middle*: 10 September, 1974 (Hiei, 1982). *Bottom*: 7 August, 1972 (Machado and Rust, 1974). In the 24 April flare each of the filled circles represents the mean of individual measurements in (typically) six bright windows contained within the first eight spectral regions listed in Table I; the three open circles are derived from Figure 6, using measurements near the minima between Balmer lines. Error bars are standard deviations of the means.

$\Delta I/I_{\text{ph}}$ with decreasing wavelength. Michard (1959) described the qualitative characteristics of WLF spectra, noting that the continuum became enhanced below 4000 Å. Machado and Rust (1974) obtained quantitative spectral data for the flare of 7 August, 1972, which showed an enhancement $(I_f - I_0)/I_0 \approx 0.02$ in the spectrum windows near 4300 Å, with a gradual increase to about 0.12 at 3550 Å (a portion of this data is reproduced in Figure 3). A distinct Balmer jump does not appear in the latter spectrum. In contrast to this, the WLF of 10 September, 1974 (Hiei, 1982) showed a relatively flat continuum down to approximately 3660 Å where the intensity increased abruptly at an advanced Balmer limit (Figure 3).

The blue enhancements inferred from the quantitative data are consistent with a number of visual observations which noted bluish colors in WLFs (see descriptions in Becker (1958), Švestka (1966b), and McIntosh (1967). Approximately half of the visually-observed WLFs, however, are described as white in color (see above references and Feibelman (1974)). Because the sensitivity of the human eye vanishes near 4000 Å and varies from one individual to another (e.g. Moon, 1961) it would not be surprising, in view of the increased contrast occurring near 4000 Å, that WLFs could appear either white or blue. Two cases of reddish or pink tints in WLFs (Martheray, 1922; Neidig and Beck, 1982) seem exceptional, and could be attributed to extremely intense emission in the $H\alpha$ line, although there is no direct evidence to support this suggestion.

3. Analysis

An inspection of the flare spectrum shows that the vast majority of photospheric lines are not in emission but, rather, appear smoothed over by the WLF continuum. A distinct

impression is obtained that the continuum is superposed on background lines which are unaffected by the flare. Such a circumstance would, indeed, be fortunate because it allows a determination of both the optical thickness $\Delta\tau_\lambda$ and the radiative source function S_λ for the continuum-emitting layer, as described below. The assumption that the background lines are not flare-affected is, of course, quite critical to such analysis, although it can be subjected to a crude test by the same procedure used to obtain S_λ and $\Delta\tau_\lambda$. The values for S_λ and $\Delta\tau_\lambda$ derived from the continuum (Section 3.1) are indicative of the low temperature (~ 6700 K), high density (hydrogen density $N_H \gtrsim 10^{16} \text{ cm}^{-3}$) conditions in the flare. Corroborating evidence for the presence of a substantial optical thickness in the Balmer continuum is provided by analysis of the Balmer lines (Section 3.2) which indicates both a high electron density ($N_e \simeq 5.3 \times 10^{13} \text{ cm}^{-3}$) and large column density of second-level hydrogen atoms ($N_2 z > 10^{16} \text{ cm}^{-2}$, where z is the flare thickness).

3.1. THE CONTINUUM

Let S_λ and $\Delta\tau_\lambda$ represent the mean values for the source function and optical thickness in a continuum-emitting layer located above the atmospheric level which produces all but the strongest photospheric lines, with the intensity of radiation incident on the layer from below given by $I_{0,\lambda}$. If S_λ and $\Delta\tau_\lambda$ are assumed constant with height in the continuum-emitting layer, then the difference ΔI_λ between the intensity $I_{f,\lambda}$ in the flare and $I_{0,\lambda}$ is easily expressed by the transfer equation:

$$\Delta I_\lambda = S_\lambda(1 - e^{-\Delta\tau_\lambda}) - (1 - e^{-\Delta\tau_\lambda})I_{0,\lambda}. \quad (1)$$

In practice, the incident intensity $I_{0,\lambda}$ cannot be obtained from the non-flaring photospheric spectrum because the flare itself may lie within the photosphere. If the flare location is limited to the upper photosphere, however, $I_{0,\lambda}$ might be sufficiently well approximated from a measurement of the non-flaring photosphere; a check for consistency in this regard is made in Section 4, after the height of the flaring layer is determined.

Equation (1) is linear in $I_{0,\lambda}$, with a slope related to $\Delta\tau_\lambda$ and an $I_{0,\lambda}$ intercept equal to S_λ . To test the linearity predicted by the basic assumption a series of measurements of $I_{f,\lambda}$ and $I_{0,\lambda}$ is obtained in a narrow region of the spectrum, over which it is safe to assume that S_λ and $\Delta\tau_\lambda$ do not vary significantly with wavelength. Figure 4 shows the result obtained between 3804 and 3823 Å (this data represents neither the best nor the worst of 16 spectral regions studied). In Figure 4 the unit of intensity is \bar{I}_0 , the intensity of the background spectrum averaged over the wavelength range considered. For $I_{0,\lambda} \gtrsim 0.5\bar{I}_0$ the variation in $\Delta I_\lambda((I_f - I_0)/\bar{I}_0)$ in Figure 4) indeed appears linear, with line cores following the same relationship as relative maxima between lines. Below $I_{0,\lambda} \simeq 0.5\bar{I}_0$ the line cores fall above the linear relationship, presumably because these stronger lines have substantial contribution functions within the flaring layer. The assumption that the background lines are unaffected by the flare is consistent with the data of Figure 4, provided that the lines in question are restricted to the linear portion of the curve (the validity of this approach is discussed further in Section 4). A linear fit

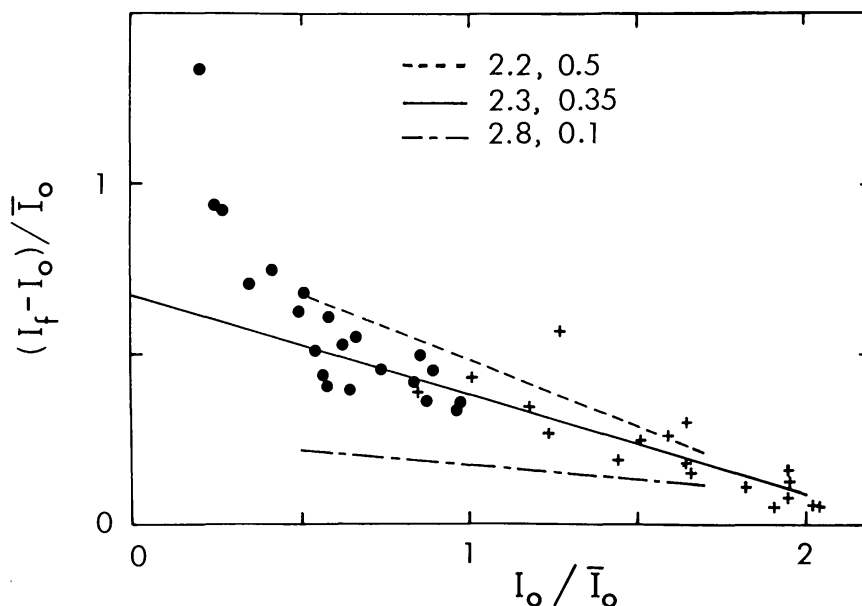


Fig. 4. Intensity differences between flare and background at a number of points in the spectrum between 3804 and 3823 Å. Dots represent the cores of absorption lines; crosses represent relative maxima between lines. \bar{I}_0 is the intensity of the non-flaring spectrum averaged over the interval 3804 to 3823 Å. The included linear relationships are as predicted for overlying continua characterized by the given values of source function (in units of \bar{I}_0) and optical thickness.

to the latter then determines the two parameters S_λ and $\Delta\tau_\lambda$. For Figure 4 the adopted values are $S_\lambda = 2.3\bar{I}_0$ and $\Delta\tau = 0.35$. The units of S_λ are converted to cgs intensity units with the aid of solar irradiance tables (e.g. Thekaekara, 1974), converted from mean to normal intensity, and corrected for limb darkening; the limb darkening functions for spectral windows (e.g., Allen, 1973) are sufficient, as the ratio $\bar{I}/I_{0, \text{window}}$ is known both at the flare location (by direct measurement) and at disk center (Allen, 1973). This procedure is then repeated to obtain 16 pairs of S_λ , $\Delta\tau_\lambda$ values at various locations in the spectrum listed in Table I. These measurements are summarized in Figure 5. Unfortunately the data become quite noisy for $\lambda \gtrsim 6000$ Å; in addition, suitable lines become so scarce that wavelength intervals as wide as 100 Å must be used in order to establish slopes and intercepts as in Figure 4. The interesting spectral region below 4000 Å, however, abounds with lines, and is contained entirely within the 3550–4550 Å range of a single third-order spectrogram.

For wavelengths longward of 4200 Å, where the emission is presumably dominated by H^- , the source function measurements are roughly equivalent to a Planck function at $T = 6700$ K. Below 4200 Å the source functions fall in the range 6000–6500 K. A smaller S_λ for Balmer continuum might be expected, due to departures from LTE, although the wavelength at which the decline occurs should then coincide with the head of the Balmer continuum, which it does not (compare Figure 3). The S_λ 's in the wavelength range 3700–4000 Å are, therefore, anomalously small, and could be due either to unidentified sources of opacity or to some error in the measurements. The same

TABLE I
Spectral regions in which source functions and optical thicknesses were measured

$\lambda_0 \pm \Delta\lambda$ (Å)	Remark
3600 ± 9.5	In Balmer continuum
3640 ± 5	In Balmer continuum
3697 ± 5	In region of merged Balmer lines
3742 ± 2.8	Between H_{12} and H_{13}
3814 ± 9.5	Between H_9 and H_{10}
3862 ± 5.5	Between H_8 and H_9
3912 ± 7.5	Between calcium K and H_8
4002 ± 4	λ_0 32 Å from $H\epsilon$
4045 ± 6.8	Approximately midway between $H\delta$ and $H\epsilon$
4085 ± 3.5	λ_0 17 Å from $H\delta$
4249 ± 19	λ_0 91 Å from $H\gamma$
4518 ± 18	
4900 ± 11	λ_0 39 Å from $H\beta$
5897 ± 13	
6544 ± 50	All data points > 20 Å from $H\alpha$
8210 ± 40	Includes points on both sides of Paschen jump

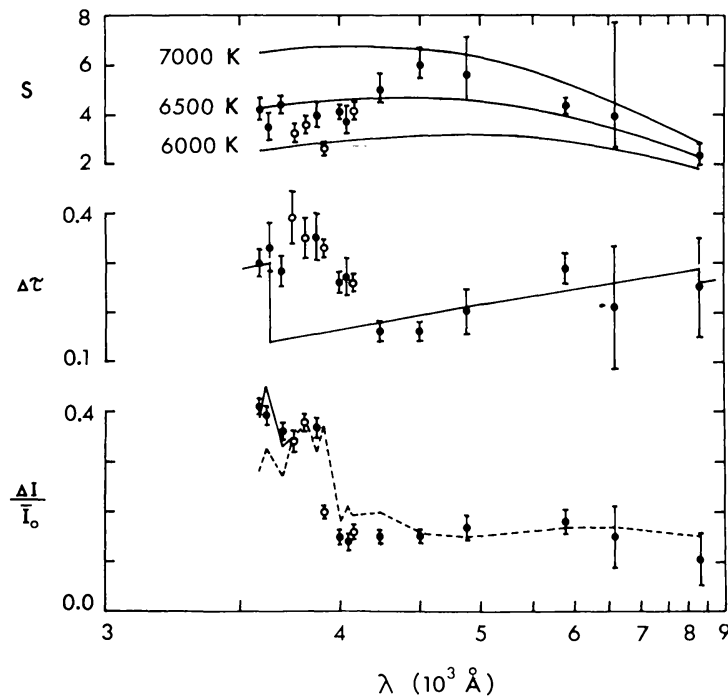


Fig. 5. *Top*: measurements of the source function in the flare continuum, compared with Planck functions for three temperatures (units are $10^6 \text{ erg s}^{-1} \text{ cm}^{-2} \text{ sr}^{-1} \text{ \AA}^{-1}$). *Middle*: measurements of the optical thickness, fitted with an opacity function for bound-free transitions of neutral and negative hydrogen (see text). *Bottom*: intensity enhancements in each of the 16 spectral regions, measured at a point where the non-flaring background intensity is equal to \bar{I}_0 (\bar{I}_0 is the intensity of the non-flaring spectrum averaged over the particular spectral region). The dashed curve is the enhancement predicted by H^- emission alone, while the solid curve represents both H^- and Balmer continuum for $\lambda \leq 3700$ Å (see text). Open circles in all three panels represent measurements which may be affected by Balmer lines.

caution applies to the $\Delta\tau_\lambda$'s which presumably display the expected jump in opacity due to the Balmer continuum but which appear anomalously large between 3700 and 4000 Å. Ignoring, for the moment, the latter spectral region we proceed to fit the $\Delta\tau_\lambda$ measurements with functions having wavelength dependences according to the absorption coefficients for the known principal contributors to the opacity, *viz.*, bound-free transitions of neutral and negative hydrogen (Gingerich, 1964; Allen, 1973). The probable extent of the opacity in the Paschen continuum, which can be estimated from the size of the Balmer opacity jump, is negligible in comparison to H^- and produces a Paschen jump too small to be detected in these data.

The bottom panel in Figure 5 shows the intensity of the flare continuum as it would appear over a background intensity equal to \bar{I}_0 , for each of the 16 spectral regions studied. Such a representation is of interest because \bar{I}_0 , the intensity averaged over a wavelength interval $\Delta\lambda$, is essentially the intensity of the photospheric background that would be observed in filters with bandpasses of similar $\Delta\lambda$. The plotted points in Figure 5 are derived from graphs analogous to Figure 4, at points on the fitted straight-line portions of the curves where $I_0/\bar{I}_0 = 1$. Due to contributions from some of the stronger lines (those with $I/\bar{I}_0 \lesssim 0.5$), however, the $\Delta I/\bar{I}_0$ values in Figure 5 will not be identical to the integrated ratios $\int_{\Delta\lambda} [(I_{f,\lambda} - I_{0,\lambda})/I_{0,\lambda}] d\lambda$ (as a check, the latter integration was actually performed for two 20 Å intervals at 3600 and 4250 Å; the resulting ratios, 0.62 and 0.16, respectively, may be compared with Figure 5 where $\Delta I/\bar{I}_0$ is found to be 0.41 and 0.15 at the same wavelengths).

It is surprising to note, in Figure 5, that a large jump in $\Delta I/\bar{I}_0$ occurs between 3860 and 4000 Å; this is in contrast to the intensity measurements made in the spectrum *windows* (Figure 3), which show a flat spectrum over the same spectral region (with a Balmer jump at 3700 Å). The distinctly different character of these two intensity plots is due to the fact that the background photospheric spectrum, with its spectral irregularities smoothed (i.e., what is essentially equal to \bar{I}_0), shows a large drop below 4000 Å due to line blanketing. This drop, however, is much less pronounced in the spectrum windows and, thus, relatively little change in the flare contrast is observed in Figure 3. When referring the flare intensity to \bar{I}_0 the relative *increase* in $\Delta I/\bar{I}_0$ below 4000 Å can actually exceed the magnitude of the relative *decrease* in the background (smoothed) photospheric spectrum at the same wavelength. This is demonstrated in Figure 5 where the data are compared with curves representing the variation of $\Delta I/\bar{I}_0$ with wavelength predicted by the transfer equation for two situations: (1) $\Delta\tau_\lambda$'s according to the fitted curve in the second panel of Figure 5, but without contribution from the Balmer continuum (the remaining opacity is mostly H^-) and S_λ 's equivalent to Planck functions B_λ (6700 K); (2) the same as (1) except for $\lambda \lesssim 3700$ Å an additional optical thickness of 0.15 representing the Balmer continuum is included and a source function $S = 4 \times 10^6 \text{ erg s}^{-1} \text{ cm}^{-2} \text{ sr}^{-1} \text{ Å}^{-1}$ (approximately as observed) is used. Note that case (1) (dashed curve) predicts an approximately 30% increase in $\Delta I/\bar{I}_0$ below 4500 Å, followed by an additional 100% increase below 4000 Å. These predicted changes in $\Delta I/\bar{I}_0$ can be compared with the corresponding intensity changes in the smoothed background solar spectrum at these wavelengths (approximately 16 and 38%, respec-

tively (Allen, 1973). The foregoing description of the flare contrast is essentially what was proposed by Švestka (1966a) as a possible explanation for the blue color of WLFs. The observed intensities, in fact, agree fairly well with H^- emission (dashed curve) down to 3700 Å, below which they follow the solid curve corresponding to Balmer continuum in addition to H^- emission (deviations from the dashed curve between 3900 and 4200 Å will be discussed in Section 4).

The source functions in the Balmer continuum (Figure 5) correspond to Planck functions $B_\lambda(T)$ at somewhat lower temperatures than those for the H^- emission. While the H^- emission is probably, to a good approximation, in LTE (Emslie and Machado, 1979), the source function for the Balmer continuum S_{BaC} is more likely given by $B_\lambda(T)/b_2$, where b_2 is the departure coefficient for second-level hydrogen atoms. Because the population states of the lower energy levels are determined primarily by the radiation field, which may be dominated by the underlying photosphere, we expect $b_2 > 1$. Since the $\Delta\tau_\lambda$'s for the H^- and Balmer continuum are small (0.15) and roughly equal in the vicinity of the Balmer jump, the observed $S_{\lambda < 3700 \text{ \AA}} \simeq 4 \times 10^6 \text{ erg s}^{-1} \text{ cm}^{-2} \text{ sr}^{-1} \text{ \AA}^{-1}$ can be approximated as the mean of S_{BaC} and S_{H^-} ; and since $S_{H^-} \simeq B_\lambda(6700 \text{ K}) \simeq 5 \times 10^6 \text{ erg s}^{-1} \text{ cm}^{-2} \text{ sr}^{-1} \text{ \AA}^{-1}$, we would then have $S_{\text{BaC}} \simeq 3 \times 10^6 \text{ erg s}^{-1} \text{ cm}^{-2} \text{ sr}^{-1} \text{ \AA}^{-1}$. Then if the electron temperature were 6700 K in the Balmer-emitting region b_2 would equal 1.6. This compares with $b_2 \simeq 2-3$ found by Švestka (1965) using population ratios derived from the analysis of Balmer lines in several flares whose electron temperatures were near 7000 K. It must be warned, however, that an electron temperature of 6700 K, even if appropriate for the H^- emission, would probably be acceptable for the Balmer continuum only in the case where both types of emission originate in the same layer of the flare. This would seem unlikely, as the Balmer continuum favors higher temperature and lower density, in comparison to H^- . It is expected, therefore, that the Balmer emission could form in a somewhat higher layer and that 6700 K might then represent a lower limit for the electron temperature in the Balmer-emitting layer of the flare.

The absorption coefficient at the head of the Balmer continuum is given by (e.g. Allen, 1973)

$$\alpha_{\text{BaC}} \simeq 1.40 \times 10^{-17} N_2 \text{ cm}^{-1}, \quad (2)$$

where N_2 is the number density (cm^{-3}) of second-level hydrogen atoms. If z is the thickness (cm) of the flaring layer along the line of sight then $\Delta\tau_{\text{BaC}} = \alpha_{\text{BaC}} z$, which, from Figure 5, is 0.15. The column density $N_2 z$ is then computed to be $1.1 \times 10^{16} \text{ cm}^{-2}$, a value which is not dependent on the assumption of a temperature in the absorbing layer.

The absorption coefficient for bound-free transitions of negative hydrogen (Gingerich, 1964), evaluated at 3646 Å and $T_e = 6700 \text{ K}$, is given by

$$\alpha_{H^-} \simeq 1.38 \times 10^{-38} N_1 N_e \text{ cm}^{-1}, \quad (3)$$

where N_1 has been substituted for the number density of neutral hydrogen atoms N_{H} . From Figure 5, $\Delta\tau_{H^-} \simeq 0.15$, which leads to $N_1 N_e z \simeq 1.1 \times 10^{37} \text{ cm}^{-5}$. Nothing further

can be derived for the continuum-emitting layer without assuming that 6700 K applies also to the Balmer continuum and that the electron density $N_e = 5.3 \times 10^{13} \text{ cm}^{-3}$ (derived in Section 3.2 from the Balmer lines) applies also to the H^- emission, i.e., assume that both types of continuum originate in the same homogenous layer. As an aside, it can be shown, under the latter assumption and using the combined Boltzmann-Saha equation and $b_2 = 1.6$, that the observed $N_2 z$ and $N_1 N_e z$ yield $b_1 = 2.5$, $N_1 = 9.3 \times 10^{16} \text{ cm}^{-3}$ (which would place the layer well within the photosphere), $N_2 = 4.9 \times 10^9 \text{ cm}^{-3}$ and $z = 22 \text{ km}$. The assumption that both emissions originate in a common layer is probably incorrect, as discussed previously; nevertheless a lower limit on N_{H} can be estimated, as shown in Section 4.

3.2. THE BALMER LINES

The profiles of the Balmer lines in flares are characterized by Stark broadening and radiation damping (e.g. Švestka, 1965), where the half-widths of the higher lines and the optical thicknesses in the wings of the lower lines can be used to determine both the electron density and column density $N_2 z$ in the flare layer. The analysis herein follows the procedure described by Švestka (1965), and begins with the measurement of the

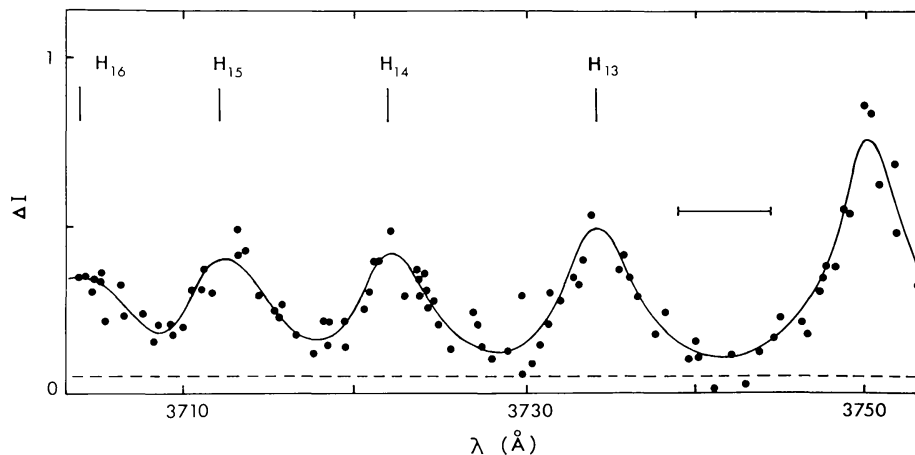


Fig. 6. Profiles of Balmer lines near the point of merging. Vertical scale is in units of the intensity of the bright spectral windows near 3742 \AA , i.e., $\Delta I = 1.0$ corresponds to $2.6 \times 10^6 \text{ erg s}^{-1} \text{ cm}^{-2} \text{ sr}^{-1} \text{ \AA}^{-1}$. Dashed line represents the baseline assumed to be 'zero intensity' for the purpose of measuring the half-widths of the lines (this baseline is chosen to be equal to the minimum $\Delta I/I_{\text{window}} (= 0.05)$ observed in Figure 3). In fitting the line profiles the locations of the emission line peaks were constrained to the theoretical Balmer center-line wavelengths. Bracket between H_{12} and H_{13} represents the wavelength range over which the opacity measurement at 3742 \AA was obtained.

half-widths of the lines H_{12} to H_{16} (Figure 6). For most large flares the half-widths reach a minimum at H_8 – H_{10} as the lines begin to become optically thin (Švestka, 1965); thereafter the widths increase with higher series number, due to the Stark effect, and the half-widths can be related to the electron density using Figure 7 of Švestka (1965). In the 24 April flare, however, the lines merge to form a continuum at approximately H_{16} , before becoming optically thin. Nevertheless, a minimum total half-width of

approximately 5 \AA occurs at H_{13} or H_{14} , while H_{15} is somewhat larger at 5.7 \AA . These widths overestimate the true half-widths, due to small contributions to the half-peak intensities from the wings of neighboring lines. A correction can be easily made, however, by substituting narrower profiles whose widths are determined by the requirement that at the relative minima the intensities in the wings of the corrected profiles must be half the observed minima. In this way a corrected half-width of 5.2 \AA is obtained for H_{15} , which implies $N_e = 6.0 \times 10^{13} \text{ cm}^{-3}$. This density must then be corrected for the effect of self-absorption in the line. The optical thickness near the center of H_{15} , as measured by the filling of the photospheric absorption lines, is 0.45 (after subtracting the contribution due to H^-). The true electron density, using the procedure described by Švestka and Fritzová-Švestková (1967), would then be 12% lower, or $5.3 \times 10^{13} \text{ cm}^{-3}$.

Once N_e has been determined, the column density $N_2 z$ can be found by measuring the optical thickness in the wings of various Balmer lines and comparing the result with Equation (67) of Švestka (1965). Using a total of 11 photospheric lines in the wings of $H\beta$, $H\gamma$, and $H\delta$, and making allowance for the contribution to the opacity by the H^- continuum, we obtain $N_2 z = 3.4 \times 10^{16} \text{ cm}^{-2}$. This value is larger than that obtained from the Balmer continuum; nevertheless it is notable that the result independently predicts a substantial optical thickness in the Balmer continuum.

Švestka (1965) describes a procedure whereby T_e and b_n ($2 \leq n \leq 8$) can be obtained from the population ratios among the various hydrogen levels as derived from measurements of the source functions in the wings of the individual Balmer lines. The success of the method, however, depends on a sufficiently rapid rate of convergence of the b_n 's. Whether due to a failure to meet the latter condition or to observational error, the method failed to converge on a set on b_n 's and T_e for the 24 April flare. Hence there is no independent assessment available for N_2 and T_e for the Balmer emission.

4. Discussion

A principal question remains regarding the anomalous opacity between 3700 and 4000 \AA . This spectral region also contains the anomalously small values for S_λ and $\Delta I/\bar{I}_0$ (Figure 5). With regard to opacity, the highly broadened Balmer lines will contribute substantially, even midway between the lines, as the point of line merging is approached. In addition, the $\Delta\tau$ measurements in Section 3.1 require wavelength intervals sufficiently large to obtain statistically significant samples of background photospheric lines; and if these intervals are appreciable fractions of the distances between adjacent Balmer lines a disproportionate contribution from line opacity would be expected (for example, see caption for Figure 6). Thus the large $\Delta\tau$'s at 3742 and 3814 \AA can be understood on the basis of one or both of these effects. Two other intervals, centered at 3912 and 4085 \AA , may also be too close to Balmer lines, and are therefore of questionable value. On the other hand, the measurements at 3862 , 4002 , and 4045 \AA , which are placed sufficiently far from Balmer lines, indicate opacity considerably in excess of what is implied for H^- alone. Thus, unless lines or other sources contribute to the opacity in

this flare, we should consider the possibility of systematic error. One example of the type of error which could produce the effects in question is the reflection by the film holder of a small fraction of the flare spectrum onto the adjacent background spectrum. If this has in fact occurred the effect must be quite subtle, as it cannot be independently confirmed in the data; hence no correction for it has been attempted. If the anomalous opacity is real then the blue continuum of WLFs is not yet understood. But, since the increase in $\Delta I/\bar{I}_0$ near 4000 \AA seems satisfactorily explained in this flare by H^- emission alone, the evidence presented here for an additional source of opacity must be considered equivocal at best. The brightenings observed at 3862 \AA (Zirin and Neidig, 1981) and at 3835 \AA (Zirin, 1980; Zirin and Tanaka, 1973) might be attributed to H^- as well, although, since these measurements were made with broad-band filters, there could have been contributions by line emissions.

The problem of the conspicuous absence of Balmer continuum in flares has been discussed by Švestka (1965). Švestka used values typical of large flares ($N_e \simeq 3 \times 10^{13} \text{ cm}^{-3}$, $N_2 z \simeq 3 \times 10^{15} \text{ cm}^{-2}$, and $T_e \simeq 7000 \text{ K}$) and concluded that the upper limit on the effective thickness of the flaring region must be only a few tens of kilometers, in order for the Balmer continuum to be undetected. The analysis of Balmer lines indicates that small effective thicknesses seem to apply to flares in general; this is true also for limb flares, suggesting that the phenomenon is not due simply to a small vertical extent of the Balmer-emitting layers (e.g. Švestka, 1965). Such observations prompted writers (e.g. Suemoto and Hiei, 1959; Švestka, 1965) to postulate flare layers of acceptably large vertical extent but which consisted of optically thin material interspersed with denser, spatially unresolved filaments; the radiation from the dense elements would then be diluted and the flare would appear to have a small effective thickness. An alternative explanation, however, might be that the electron densities in flares have been systematically overestimated due to the line broadening effects of strong electric fields generated in flare plasmas (Spicer and Davis, 1975; Davis, 1977). If correct, the fictitiously large electron density would have a rather potent effect on the calculated flare thickness, as the latter is ordinarily obtained by dividing the observed $N_2 z$ by a calculated density N_2 which varies as N_e^2 .

With regard to the energy source for the optical continuum it is of particular interest to know the height in the atmosphere where the emission occurs. Because most of the energy in the continuum of the 24 April flare is radiated by H^- , with a probable electron temperature of 6700 K , it seems appropriate to consider the height where this temperature is usually attained in flares. Generally, model atmosphere calculations indicate the following effects of the flare on the atmosphere: the height (above $\tau_{5000} = 1$) of the temperature minimum is lowered from 500 km to about 300 km ; the minimum temperature is increased from 4200 to about 5000 K ; the temperature gradient in the chromosphere is steepened (Hénoux and Nakagawa, 1977; Brown *et al.*, 1978; Lites and Cook, 1979; Dinh, 1980; Machado *et al.*, 1980). The published models, which apply to far less spectacular flares, place the 6700 K level at heights in the range $600\text{--}1000 \text{ km}$, where $N_{\text{H}} \sim 10^{14} \text{ cm}^{-3}$. By comparison, $N_{\text{H}} \simeq 9.3 \times 10^{16} \text{ cm}^{-3}$ (corresponding to $h \simeq 50 \text{ km}$ (Vernazza *et al.*, 1981) was derived in Section 3.1 by assuming, probably

incorrectly, a common layer for both H^- and Balmer continuum. Nevertheless, if N_e is taken as a free parameter in the H^- emitting (6700 K) region it remains impossible to obtain N_H less than approximately $1.6 \times 10^{16} \text{ cm}^{-3}$ for any reasonable choices of b_1 ($\lesssim 18$) and z ($\lesssim 300 \text{ km}$) that could result in the observed value for $N_1 N_e z$ (the selected N_e is then $1-2 \times 10^{13} \text{ cm}^{-3}$). Furthermore, there is an additional constraint that in selecting smaller values for N_H the resulting calculated values for $N_2 z$ within the H^- emitting layer must not exceed, under reasonable choices for b_2 , the total observed $N_2 z$. In this way $N_H \simeq 1.6 \times 10^{16} \text{ cm}^{-3}$ is estimated as the lower limit for the density in the H^- emitting layer. Unless atmospheric compression plays a role in achieving this density, it indicates an upper limit of approximately 300 km for the height of the layer (Vernazza *et al.*, 1981), which corresponds to a total atmospheric mass column density $\gtrsim 0.4 \text{ g cm}^{-2}$.

The height of the lower boundary of the flare can be estimated by noting the effect of the flare on lines with known heights of formation in the non-flaring atmosphere. This method will work for lines whose contribution functions behave approximately as in LTE, such as the Fe I lines studied by Lites (1972). Table II lists a number of these lines along with a measurement of the flare effect on each. It is seen that lines formed above approximately 300 km are strongly flare affected, while those formed entirely below 200 km show enhancements which can be accounted for by the continuum alone (the continuum contribution was computed using B_λ (6700 K), $\Delta\tau_\lambda$ according to the fitted opacity curve in Figure 5, and I_0 from the measurements in Table II). Machado and Rust (1974) employed a similar technique in order to determine the maximum depth of

TABLE II
Flare effect on Fe I lines studied by Lites (1972)

$\lambda(\text{\AA})$	$h_{\tau=1}(\text{km})^a$	$(h_{\text{upper}}, h_{\text{lower}})^b$	I_0/I_c^c	ΔI^d
3820.4	794	1086, 592	0.09	1.67
4271.8	564	832, 341	0.10	0.86
5269.6	445	675, 271	0.16	1.61
5227.2	299	637, 141	0.21	1.46
5233.0	165	456, 47	0.22	0.61
4602.9	86	238, -21	0.36	-0.11
5123.7	53	193, -263	0.41	0.35
5250.2	-54	116, -228	0.52	0.08
6430.9	-42	96, -124	0.73	-0.08

^a Height at which $\tau_{5000} = 1$ in the line, at 60 degrees from disk center (listed height is the mean over a width of the line core corresponding to the spectrograph resolution).

^b Height range containing 90% of the emergent line radiation (corrected for spectrograph resolution) at 60 degrees from disk center.

^c Intensity of the line relative to the local continuum, measured from the non-flaring spectrum.

^d Amount by which the difference in the line intensity, as measured inside and outside the flare, exceeds the intensity enhancement in the line due to filling by flare continuum alone (in units of $10^6 \text{ erg s}^{-1} \text{ cm}^{-2} \text{ sr}^{-1} \text{ \AA}^{-1}$).

flare emission in the WLF of 7 August, 1972. They compiled a list of more than 400 lines of various elements, and, although the data were qualitative, concluded that the flare did not penetrate deeper than 200 km.

The method of analysis in Section 3.1 depends critically upon the assumption that the flaring layer is located above the layers in which the weaker photospheric lines are formed. The validity of this assumption is based on several arguments. First, the observed relationship between $I_f - I_0$ and I_0 (for example, Figure 4) is linear in all 16 spectral regions studied; this is consistent with the prediction of the transfer equation for simple absorption and emission in an overlying layer. However, this is only a requirement that the assumption must fulfill and does not rule out the possibility of an atmospheric temperature structure producing a similar effect. The latter situation, however, seems doubtful because the slopes of the linear portions of the $I_f - I_0$ vs I_0 plots obtained in 16 separate spectral regions differ significantly from one another (this is true whether relative or absolute intensities are plotted); and, because the spectrum lines used to determine the slopes were chosen at random, it would seem unlikely that a single atmospheric solution would fit all slopes simultaneously. Finally, for a given plot such as Figure 4 the enhancements $I_f - I_0$ for lines are continuous with (and even overlap) those for relative maxima between lines; this suggests that it is simply the intensity I_0 of the background point that is related to $I_f - I_0$, for a given S_λ and $\Delta\tau_\lambda$.

A correlation between $I_f - I_0$ and I_0 was not found in the 12 March, 1969 WLF spectrum studied by Machado (1971). Neither is there a simple relationship between $I_f - I_0$ and I_0 which applies simultaneously to both line cores and windows for the 10 September, 1974 WLF (Hiei, 1982). In both cases, however, the authors concluded that the continuum originated in the photosphere; and if the flare were distributed throughout the line forming region, correlations such as Figure 4 would not be expected.

The conclusion of the discussions above is that the H^- emission originates between the height limits 200–300 km. At the lower limit of this range the optical depth at 5000 Å in the continuum of the non-flaring atmosphere is approximately 0.05 (Vernazza *et al.*, 1981), which, at $T \lesssim 5000$ K, would contribute less than 1.5% of the total photospheric continuum intensity. Thus the intensity in the spectrum outside the flare is a sufficiently good approximation to the intensity $I_{0,\lambda}$ incident on the bottom of the flare layer (as assumed in Equation (1)), insofar as the continuum windows are concerned. As for the case of lines it should at least be assured that the height range contributing most of the emergent radiation lies well below the 200 km level. Data on the heights of formation are not available for the vast majority of the lines used in the analysis, although, if Table II can be taken as an indication, lines which lie on the linear portions of curves such as Figure 4 (those with $I_0/I_c \gtrsim 0.30$) do appear to satisfy the condition.

5. Energetics

The results of Section 3 are based on measurements obtained three arcsec from the brightest point in the flare kernel. It is interesting to compare the radiative output in the continuum at this location with that radiated in $H\alpha$. Using a Planck function at 6500 K,

an opacity according to Figure 5, and assuming that the same contributors to the opacity apply beyond the wavelength range of the measurements, it follows that the continuum must be contained almost entirely between 2000 and 16000 Å. Integration of Equation (1) over this range then gives $9.5 \times 10^9 \text{ erg s}^{-1} \text{ cm}^{-2}$ for the continuum alone. This is compared with $1.5 \times 10^8 \text{ erg s}^{-1} \text{ cm}^{-2}$ obtained by integrating in wavelength over the H α line at the same point in the flare. The factor of approximately 60 between these values is in good agreement with earlier comparisons made by Slonim and Korobova (1975).

With regard to the mechanism which heats the continuum-emitting layer, it is noted that the radiative output of $9.5 \times 10^9 \text{ erg s}^{-1} \text{ cm}^{-2}$, if contributed over a path length of 100 km, implies a large loss rate of $10^3 \text{ erg s}^{-1} \text{ cm}^{-3}$; and this rate applies at a location in the flare where the brightness is only 25% of the maximum. The rate of energy deposition by high energy ($\geq 10 \text{ MeV}$) protons at heights $\leq 300 \text{ km}$ might fall short of this, however, as Hudson and Dwivedi (1982) have obtained $\lesssim 60 \text{ erg s}^{-1} \text{ cm}^{-3}$ from observed gamma-ray fluxes in the WLF of 11 July, 1978 (gamma-ray data were not available for the 24 April flare).

The source function, optical thickness, and relative contribution by flare-excited lines remain unknown at the brightest point in the kernel. Nevertheless, the radiative output (lines and continuum) can be estimated by noting that the MBP measurements suggest an overall spectral shape similar to the result of Figure 5. Using this fact, an output of approximately $3.6 \times 10^{10} \text{ erg s}^{-1} \text{ cm}^{-2}$ is obtained. The output integrated over the entire kernel is estimated from the product of the latter value and the area of the kernel within its half-intensity points (approximately $1.7 \times 10^{17} \text{ cm}^2$). The result is $6.1 \times 10^{27} \text{ erg s}^{-1}$. The total energy output, obtained by integrating over time, is difficult to estimate because of complex variations in several additional kernels appearing before and after the time of peak brightness. A conservative estimate, however, is $6 \times 10^{29} \text{ erg}$. This value is typical of other WLFs studied in the references quoted herein.

Acknowledgements

It is a pleasure to acknowledge discussions with R. Canfield, L. Cram, E. Hiei, H. Hudson, B. Lites, D. Mihalas, D. Rust, and H. Zirin relating to the observations of this flare. A. Poland assisted in the use of the PDS microphotometer at Goddard Space Flight Center; additional measurements were made with a Joyce-Loebl microdensitometer on loan from Kitt Peak National Observatory. The observation of this flare was secured as a result of persistent efforts by L. Gilliam.

References

- Allen, C. W.: 1973, *Astrophysical Quantities*, Athlone Press, London.
 Becker, U.: 1958, *Z. Astrophys.* **46**, 168.
 Brown, J. C., Canfield, R. C., and Robertson, M. N.: 1978, *Solar Phys.* **57**, 399.
 Davis, W. D.: 1977, *Solar Phys.* **54**, 139.
 DeMastus, H. L. and Stover, R. R.: 1967, *Publ. Astron. Soc. Pacific* **79**, 615.

- Dinh, Q.-V.: 1980, *Publ. Astron. Soc. Japan* **32**, 515.
- Ellison, M. A.: 1946, *Monthly Notices Roy. Astron. Soc.* **106**, 500.
- Ellison, M. A. and Conway, M.: 1950, *The Observatory* **70**, 77.
- Emslie, A. G. and Machado, M. E.: 1979, *Solar Phys.* **64**, 129.
- Feibelman, W. A.: 1974, *Solar Phys.* **39**, 409.
- Gingerich, O.: *Harvard-Smithsonian Conference on Stellar Atmospheres*, S.A.O. Special Report No. 167, Smithsonian Astrophysical Observatory, Cambridge, Mass., U.S.A.
- Hénoux, J.-C. and Nakagawa, Y.: 1977, *Astron. Astrophys.* **57**, 105.
- Hiei, E.: 1982, *Solar Phys.* **80**, 113.
- Hudson, H. S.: 1972, *Solar Phys.* **24**, 414.
- Hudson, H. S. and Dwivedi, B. N.: 1982, *Solar Phys.* **76**, 45.
- Jefferies, J. T. and Orrall, F. Q.: 1961, *Astrophys. J.* **133**, 946.
- Lin, R. P. and Hudson, H. S.: 1976, *Solar Phys.* **50**, 153.
- Lites, B. W.: 1972, Thesis, Univ. Colorado, High Altitude Observ. Res. Memorandum No. 185, Boulder, Colo., U.S.A.
- Lites, B. W. and Cook, J. W.: 1979, *Astrophys. J.* **228**, 598.
- Machado, M. E.: 1971, *Solar Phys.* **17**, 389.
- Machado, M. E., Avrett, E. H., Vernazza, J. E., and Noyes, R. W.: 1980, *Astrophys. J.* **242**, 336.
- Machado, M. E. and Rust, D. M.: 1974, *Solar Phys.* **38**, 499.
- Martheray, M.: 1922, *Astronomie* **36**, 276.
- McIntosh, P. S.: 1967, *Sky and Telescope* **34**, 57.
- McIntosh, P. S. and Donnelly, R. E.: 1972, *Solar Phys.* **23**, 444.
- Michard, R.: 1959, *Ann. Astrophys.* **22**, 887.
- Moon, P.: 1961, *The Scientific Basis of Illuminating Engineering*, Dover Publ. Co., New York, U.S.A.
- Najita, K. and Orrall, F. Q.: 1970, *Solar Phys.* **15**, 176.
- Neidig, D. F. and Beck, R. O.: 1982, *Solar Phys.* **78**, 225.
- Rust, D. M. and Hegwer, F.: 1975, *Solar Phys.* **40**, 141.
- Slonim, Y. M. and Korobova, Z. B.: 1975, *Solar Phys.* **40**, 397.
- Spicer, D. S. and Davis, J.: 1975, *Solar Phys.* **43**, 107.
- Suemoto, Z. and Hiei, E.: 1959, *Publ. Astron. Soc. Japan* **11**, 185.
- Švestka, Z.: 1965, *Adv. Astron. Astrophys.* **3**, 119.
- Švestka, Z.: 1966a, *Bull. Astron. Inst. Czech.* **17**, 137.
- Švestka, Z.: 1966b, *Space Sci. Rev.* **5**, 388.
- Švestka, Z.: 1970, *Solar Phys.* **13**, 471.
- Švestka, Z.: 1976, *Solar Flares*, D. Reidel Publ. Co., Dordrecht, Holland.
- Švestka, Z. and Fritžová-Švestková, L.: 1967, *Solar Phys.* **2**, 75.
- Thekaekara, M. P.: 1974, *Appl. Opt.* **13**, 518.
- Vernazza, J. E., Avrett, E. H., and Loeser, R.: 1981, *Astrophys. J. Suppl.* **45**, 635.
- Waldmeier, M.: 1958, *Z. Astrophys.* **46**, 92.
- Zirin, H.: 1980, *Astrophys. J.* **235**, 618.
- Zirin, H. and Neidig, D. F.: 1981, *Astrophys. J.* **248**, L45.
- Zirin, H. and Tanaka, K.: 1973, *Solar Phys.* **32**, 173.